Available online at www.sciencedirect.com
ScienceDirect
International Journal of Heat and Mass Transfer 50 (2007) 2924–2935
International Journal of HEAT and MASS TRANSFER
www.elsevier.com/locate/ijhmt

Effects of variable density on response of spherical diffusion flames under rotation

S.W. Yoo, C.K. Law *

Department of Mechanical and Aerospace Engineering, Princeton University, Princeton, NJ 08544, United States

Received 9 November 2006; received in revised form 18 December 2006
Available online 13 March 2007

Abstract

The spherical diffusion flame generated by either a porous burner or a fuel droplet in response to rotational motion was investigated through perturbation analysis, with emphasis on the effects variable density. While it was shown that main feature of the problem was adequately described by the constant-density model, the variable-density formulation revealed two new insights: (1) perturbations due to rotation decrease substantially as compared with the constant-density formulation, suggesting that the perturbing effects of rotation are substantially absorbed and thereby mitigated by the density variation, and (2) magnitude of the perturbations strongly depends on the ratio of the burner/droplet surface temperature to the ambient temperature.

Keywords: Combustion; Rotating sphere; Asymptotic analysis

1. Introduction

The laminar flamelets constituting a turbulent flame ensemble are subjected to flow motions of a highly complex nature. Consequently, it is useful to understand the characteristics of the flame–flow interaction through various elemental phenomena such as the counterflow flame [1] and the interaction of a planar flame with a vortex [2]. An elemental configuration that has not been sufficiently studied is the spherical flame situated in a rotating flow field that is self-generated by its fuel source, as would be the situation involving the diffusional burning of spinning fuel droplets and particles. At the fundamental level, the well-controlled nature of the flame-flow configuration allows accurate quantification of the influence of the induced flow field on the extent of the flame distortion and possible extinction. Indeed, this is one of the motivations for the undertaking of microgravity experiments on burner-generated spherical flames, with and without spinning of the burner [3].

Extensive investigations have been conducted on the flow pattern and its instabilities surrounding a rotating body without combustion [4–9]. Corresponding studies involving combustion, however, have been rather limited. Specifically, Pearlman and Sohrab [10] experimentally showed that rotation enhances the vaporization of heptane droplets in normal gravity, while Lozinski and Matalon [11,12] theoretically demonstrated the same result for the pure vaporization and burning of a spinning fuel droplet with unity Lewis number, Le. This work has been recently extended to include general Le's [13], with the results that, for a moderate range of the ambient oxygen mass fraction, the flame experiences a temperature reduction at the poles but an increase at the equator when $Le_F > 1$ or $Le_O < 1$, while the response is reversed when Le is flipped such that $Le_F < 1$ or $Le_O > 1$, where the subscripts F and O, respectively, designate the fuel and oxidizer. The characteristics of flame extinction caused by rotation were also studied by analyzing the flame structure, and it was shown that the flame temperature perturbation due to rotation could lead to local extinction because of the temperature-sensitive Arrhenius kinetics. These theoretically predicted influences of Le were found to largely corroborate the microgravity

* Corresponding author. Tel.: +1 609 258 5271; fax: +1 609 258 6233.
E-mail address: cklaw@princeton.edu (C.K. Law).

0017-9310/$ - see front matter © 2007 Elsevier Ltd. All rights reserved.
doi:10.1016/j.ijheatmasstransfer.2006.12.014

Nomenclature

$'$	prime denote dimensional quantities
B'	frequency factor of chemical reaction rate, s^{-1}
c'_p	specific heat of mixture at constant pressure, J/kg/mol
Da	system Damköhler number
D'_i	molecular diffusivity of species i, m^2/s
E'	activation energy, J/mol
L	latent heat of vaporization divided by $c'_p T'_\infty$
Le_i	Lewis number of the species i, $Le_i = \alpha'/D'_i$
M	dimensionless mass flow rate
m	dimensionless mass flux
R'	radius of the droplet/burner, m
p'	pressure, Pa
Pr	Prandtl number, $Pr = \mu'/\rho'\alpha'$
R°	gas constant, J/mol/K
q'	heat of combustion per unit mass of the fuel, J/kg
T'	temperature, K
u'	radial velocity, m/s
v'	tangential velocity in zenith coordinates, m/s
W'_i	molecular weight of species i, g/mol
w'	tangential velocity in azimuth coordinates, m/s
Y_i	mass fraction of the species i

Greek symbols

α'	thermal diffusivity of the mixture, m^2/s
v_i	stoichiometric coefficient of species, i
ρ'	density of mixture, kg/m^3
σ	stoichiometric oxidizer-to-fuel mass ratio
μ'	dynamic viscosity, kg/m/s
Ω'	angular velocity of droplet/burner, s^{-1}
ω	dimensionless angular velocity, $\omega = \Omega' R'^2/\alpha'$

Subscripts

$0, 1, \ldots$	order of the perturbed solutions
f	condition at the leading-order flame location
F	relates to the fuel mixture
O	relates to the oxidizer mixture
s	condition at the surface of the burner/droplet
∞	condition at the ambient

experimental observations of spherical diffusion flames under large rotational velocities [3].

In [13] constant density was assumed for simplicity of analysis, hence allowing decoupling of the flow from thermal effects. Density variation, however, is significant because of the large and localized exothermicity of chemical reactions associated with combustion processes. Specifically, since the flame temperature of hydrocarbons burning in room-temperature air typically exceeds 2000 K, the density of the flow field can vary by factors of six to seven. Consequently, the constant-density assumption is expected to lead to grossly inaccurate predictions of the combustion phenomenon under study. For example, Klajn and Oppenheim [14] specifically addressed this issue by deriving analytic solutions for gaseous jet diffusion flames in a manner that the influence of density variation due to heat release is expressed explicitly. When compared with available microgravity experimental data, their results show that the constant-density formulation indeed overpredicts the flame size significantly.

The issue of constant density is somewhat more subtle for the present problem. That is, since the unperturbed, leading-order problem is that of the 1D spherical diffusion flame for which variable-density treatment can be readily incorporated, the constant-density assumption is made only to the perturbed, higher-order solutions [13]. Thus superficially it seems that the flame location, based on the leading-order solution, can be determined fairly accurately even with the constant-density assumption applied to the higher-order solutions. The subtlety here is that since we are mainly interested in the effects of perturbation due to rotation on the flame response, and at this level the constant-density assumption is expected to exert an O(1) influence, the coupling between the flow and density variations is expected to be strong and its nature is not clear. This therefore constitutes the primary objective of the present study, namely to extend the previous investigation [13] to allow for variable density. Since analytical solution for the perturbed flow is no longer attainable, the solution will be sought numerically and compared with that obtained from the constant-density formulation.

2. Problem formulation

As shown schematically in Fig. 1, we consider a diffusion flame supported by the inwardly transported oxidizer gas

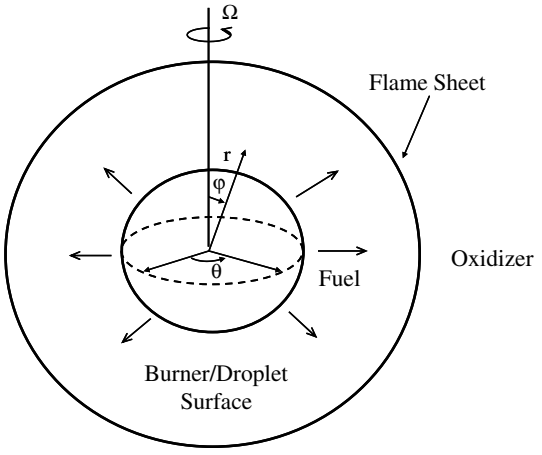

Fig. 1. Schematic of the spherical coordinate system.

and the outwardly transported fuel gas generated from either a rotating spherical porous burner (or a fuel droplet). Spherical polar coordinates (r, ϕ, θ), are employed, with the origin, $r = 0$, located at the center of the burner or droplet. The burner or droplet rotates about the axis, $\phi = 0$, at a fixed angular velocity Ω' such that the tangential velocity is $v' = \Omega' R' \sin\phi$, where R' is the radius of the burner. Axisymmetry then implies that $\partial/\partial\theta = 0$. Fuel is uniformly supplied at a constant rate from the surface of the fuel source.

The governing equations are similar to those in [12], and the effects of non-equidiffusion are considered similarly as those in [13]. Here we non-dimensionalize distance by R' and time by $(R'^2/\alpha')(\rho'_1/\rho'_\infty)$, where α' is the thermal diffusivity of the mixture in the far-field and the introduction of the liquid-to-gas density ratio is only necessary for droplet burning, which allows the quasi-steady approximation for the gas-phase process [15]. Furthermore, the temperature and density of the mixture are scaled with their far-field values, T'_∞ and ρ'_∞, while velocities are non-dimensionalized by the thermal diffusion velocity α'/R'. Since the gas velocities are typically small compared to the speed of sound, the process is thermodynamically isobaric, while the dynamic pressure deviation from the ambient value p'_∞ is non-dimensionalized by $\rho'_\infty(\alpha'/R')^2$. Finally, the mass fractions of fuel, Y_F, and oxidizer, Y_O, are scaled by $Y_{F,s}$ and $\sigma Y_{F,s}$, respectively, where the subscript "s" denotes the prescribed condition at the fuel surface. Thus the steady dimensionless conservation equations for mass, momentum, temperature and species are:

$$\nabla\cdot(\rho\mathbf{v}) = 0, \tag{1}$$

$$\rho\mathbf{v}\cdot\nabla\mathbf{v} = -\nabla p + Pr\left(\nabla^2\mathbf{v} + \frac{1}{3}\nabla(\nabla\cdot\mathbf{v})\right), \tag{2}$$

$$\rho\mathbf{v}\cdot\nabla T = \nabla^2 T + qDa\rho^2 Y_F Y_O \exp(-T_a/T), \tag{3}$$

$$\rho\mathbf{v}\cdot\nabla Y_i = Le_i^{-1}\nabla^2 Y_i - Da\rho^2 Y_F Y_O \exp(-T_a/T), \tag{4}$$

$$\rho T = 1, \tag{5}$$

where $i = $ O or F and $\mathbf{v} = (u, v, w)$ is the velocity vector. The parameter Da is the system Damköhler number:

$$Da = \left(\frac{B' Y_{F,s} W'_O v_O}{W'_F W'_O}\right)\left(\frac{\rho'_\infty R'^2}{\alpha'}\right).$$

The remaining parameters include the Lewis numbers $Le_i = \alpha'/D'_i$, the Prandtl number $Pr = \mu'/\rho'\alpha'$, the heat release parameter $q = q' Y^2_{F,s}/c'_p T'_\infty$, and $T_a = E'/R^\circ T'_\infty$ is the non-dimensional activation energy.

At the burner or droplet surface, $r = 1$, the temperature is prescribed and the flux of fuel is the balance between convection and diffusion, written as

$$w = \omega\sin\phi, \quad v = 0, \quad T = T_s, \quad mY_F - Le_F^{-1}\frac{\partial Y_F}{\partial r} = m, \tag{6}$$

where $\omega = \Omega' R'^2/\alpha'$ is the ratio of the tangential velocity to the radial diffusion velocity, and $m = \rho u$ is the radial mass flux. In the far field, $r \to \infty$ the following conditions are imposed:

$$\vec{\mathbf{v}} \to 0, \quad T \to 1, \quad Y_F \to 0, \quad Y_O \to Y_{O,\infty}. \tag{7}$$

For droplet burning, the heat transfer boundary condition is required for the determination of the vaporization rate at the surface:

$$\frac{\partial T}{\partial r} = mL. \tag{8}$$

By further assuming reaction-sheet combustion [15], the reaction terms are replaced by the jump conditions across the flame sheet, $r = r_f(\phi)$, namely

$$[T] = [Y_F] = [Y_O] = 0, \tag{9}$$

$$\left[\frac{\partial T}{\partial n} + Le_F^{-1}\frac{\partial Y_F}{\partial n}\right] = \left[\frac{\partial T}{\partial n} + Le_O^{-1}\frac{\partial Y_O}{\partial n}\right] = 0, \tag{10}$$

where n is the normal vector relative to the flame surface, and we have used the notation $[Z] = Z(r_f^+) - Z(r_f^-)$. The continuity of temperature and hence of density implies that velocities are also continuous across the reaction sheet. The jump conditions, corresponding to continuity of the tangential velocity components, as well as conservation of mass and momentum, are, respectively, given by

$$\begin{aligned}&\left[\frac{\partial}{\partial n}(\mathbf{n}\times\mathbf{v})\right] = 0,\\ &[\mathbf{v}] = 0,\\ &\left[-p + \frac{4}{3}Pr\frac{\partial}{\partial n}(\mathbf{n}\cdot\mathbf{v})\right] = 0.\end{aligned} \tag{11}$$

For small rates of rotation, $\omega \ll 1$, we construct solutions in the same manner as that discussed in [11]. All variables are expanded in series of even powers of ω such as

$$T = T_0 + \omega^2 T_2 + \omega^4 T_4 + \cdots,$$

with the exception of w, which is expanded as

$$w = \omega w_1 + \omega^3 w_3 + \cdots$$

The subscript "0" denotes the leading-order solution, describing spherically symmetric burning in the absence of rotation. The solutions for the flow field, temperature, and species mass fractions are:

$$m_0 = \frac{M_0}{r^2}, \tag{12}$$

$$v_0 = 0, \tag{13}$$

$$T_0^- = T_s + \frac{1 - T_s - q + q\exp(M_0/r_{f,0})}{\exp(M_0) - 1}[\exp(M_0 - M_0/r) - 1], \tag{14}$$

$$T_0^+ = 1 + \left[\frac{1 - T_s - q + q\exp(M_0/r_{f,0})}{1 - \exp(-M_0)} - q\exp(M_0/r_{f,0})\right] \times [\exp(-M_0/r) - 1], \tag{15}$$

$$Y_{F,0} = Y_{F,0}^- = 1 - \exp[Le_F M_0(1/r_{f,0} - 1/r)], \tag{16}$$

$$Y_{O,0} = Y_{O,0}^+ = \exp(Le_O M_0/r_{f,0} - Le_O M_0/r) - 1, \tag{17}$$

where the leading-order flame location is given by:

$$r_{\mathrm{f},0} = \frac{Le_{\mathrm{O}} M_0}{\ln(1 + Y_{\mathrm{O},\infty})}$$

and

$$u_0 = \frac{m_0}{\rho_0}, \quad \rho_0 T_0 = 1.$$

For droplet burning, the leading-order burning rate is:

$$M_0 = \ln\left(1 + \frac{1 - T_{\mathrm{s}} - q + q(1 + Y_{\mathrm{O},\infty})^{1/Le_{\mathrm{O}}}}{L}\right), \tag{18}$$

whereas M_0 is prescribed for burner-supported combustion.

To assess the influence of the rotational flow, we first solve the ϕ-component of the momentum equation, which is decoupled from the remaining components. The solution for w_1 is readily obtained as [11]:

$$w_1 = \frac{f(r)}{f(1)} \sin\phi = \bar{w}_1(r) \sin\phi, \tag{19}$$

where

$$f(r) = 2r \exp\left(-\frac{M_0}{rPr}\right) - 2r + \frac{2M_0}{Pr} - \left(\frac{M_0}{Pr}\right)^2 \frac{1}{r}. \tag{20}$$

At $\mathrm{O}(\omega^2)$, we obtain a system of linear partial differential equations with nonhomogeneous source terms driven by the centrifugal acceleration produced by $\bar{w}_1$. The form of the source suggests that we look for solutions of the form:

$$u_2 = \bar{u}_2(r) P_2(\cos\phi), \tag{21}$$

$$v_2 = \bar{v}_2(r) \frac{\partial}{\partial\phi} P_2(\cos\phi), \tag{22}$$

$$p_2 = -\frac{2}{3} \int_0^\infty \frac{\bar{w}_1^2}{r}\, \mathrm{d}r + \bar{p}_2(r) P_2(\cos\phi), \tag{23}$$

$$T_2^{\pm} = \overline{T}_2^{\pm}(r) P_2(\cos\phi), \tag{24}$$

$$Y_{\mathrm{F},2} = \overline{Y}_{\mathrm{F},2}(r) P_2(\cos\phi), \quad Y_{\mathrm{O},2} = \overline{Y}_{\mathrm{O},2}(r) P_2(\cos\phi), \tag{25}$$

$$r_{\mathrm{f},2} = \bar{r}_{\mathrm{f},2} P_2(\cos\phi), \quad T_{\mathrm{f},2} = \overline{T}_{\mathrm{f},2} P_2(\cos\phi), \tag{26}$$

where $P_2(\cos\phi) = (3\cos^2\phi - 1)/2$ is the second Legendre polynomial. Note that $P_2(\cos\phi)$ is positive at the poles ($\phi = 0, \pi$) and negative at the equator ($\phi = \pi/2$). Thus the nature of the response to rotation for the poles and equator will always be opposite to each other. For example, if $r_{\mathrm{f},2}$ is negative, it follows from Eq. (26) that the flame will deform inward toward the burner at the poles and protrude out along the equator.

When Eqs. (21)–(26) are substituted into the $\mathrm{O}(\omega^2)$ problem, the system of partial differential equations are simplified to a system of strongly coupled ordinary differential equations in r consisting of the following:

$$\frac{1}{r} \frac{\partial(r^2 \bar{m}_2)}{\partial r} - 6\rho_0 \bar{v}_2 = 0, \tag{27}$$

$$m_0 \frac{\partial \bar{u}_2}{\partial r} + \frac{\partial u_0}{\partial r} \bar{m}_2 + \frac{\partial \bar{p}_2}{\partial r} + Pr\left(-\frac{4}{3}\frac{\partial^2 \bar{u}_2}{\partial r^2} - \frac{8}{3r}\frac{\partial \bar{u}_2}{\partial r} + \frac{26}{3r^2}\bar{u}_2 + \frac{2}{r}\frac{\partial \bar{v}_2}{\partial r} - \frac{14}{3}\frac{\bar{v}_2}{r^2}\right) = -\frac{2\rho_0 \bar{w}_1^2}{3r}, \tag{28}$$

$$m_0 \frac{\partial \bar{v}_2}{\partial r} + m_0 \frac{\bar{v}_2}{r} + \frac{\bar{p}_2}{r} + Pr\left(-\frac{\partial^2 \bar{v}_2}{\partial r^2} - \frac{2}{r}\frac{\partial \bar{v}_2}{\partial r} + \frac{8\bar{v}_2}{r^2} - \frac{1}{3r}\frac{\partial \bar{u}_2}{\partial r} - \frac{8}{3}\frac{\bar{u}_2}{r^2}\right) = -\frac{\rho_0 \bar{w}_1^2}{3r}, \tag{29}$$

$$m_0 \frac{\partial \overline{T}_2}{\partial r} + \frac{\partial T_0}{\partial r} \bar{m}_2 - \frac{1}{r^2}\frac{\partial}{\partial r}\left(r^2 \frac{\partial \overline{T}_2}{\partial r}\right) + \frac{6}{r^2}\overline{T}_2 = 0, \tag{30}$$

$$m_0 \frac{\partial \overline{Y}_{i,2}}{\partial r} + \frac{\partial Y_{i,0}}{\partial r} \bar{m}_2 - \frac{1}{Le_i}\left[\frac{1}{r^2}\frac{\partial}{\partial r}\left(r^2 \frac{\partial \overline{Y}_{i,2}}{\partial r}\right) - \frac{6}{r^2}\overline{Y}_{i,2}\right] = 0, \tag{31}$$

$$\rho_0 \overline{T}_2 + T_0 \bar{\rho}_2 = 0, \tag{32}$$

$$\bar{m}_2 = \rho_0 \bar{u}_2 + u_0 \bar{\rho}_2. \tag{33}$$

Also note that $\bar{m}_2$ is zero for the burner-supported combustion, which also applies to the following boundary conditions.

The boundary conditions at the surface, $r = 1$, are:

$$\bar{v}_2 = 0, \tag{34}$$

$$\overline{T}_2 = 0, \tag{35}$$

$$\frac{1}{Le_{\mathrm{F}}}\frac{\partial \overline{Y}_{\mathrm{F},2}}{\partial r} = -\bar{m}_2(1 - Y_{\mathrm{F},0}) + m_0 \overline{Y}_{\mathrm{F},2}. \tag{36}$$

For droplet burning, we have

$$\frac{\partial \overline{T}_2}{\partial r} = \bar{m}_2 L, \tag{37a}$$

whereas the mass flux is prescribed for the burner-supported combustion:

$$\bar{u}_2 = 0. \tag{37b}$$

The jump conditions at the leading-order flame location, $r = r_{\mathrm{f},0}$, are:

$$\left[\bar{u}_2 + \bar{r}_{\mathrm{f},2}\frac{\partial u_0}{\partial r}\right] = 0, \tag{38}$$

$$\left[\bar{v}_2 + \bar{r}_{\mathrm{f},2}\frac{\partial v_0}{\partial r}\right] = 0, \tag{39}$$

$$\left[\frac{\partial}{\partial r}\left(\bar{v}_2 + \frac{\bar{r}_{\mathrm{f},2}}{r_{\mathrm{f},0}} u_0\right)\right] = 0, \tag{40}$$

$$\left[\bar{p}_2 + \bar{r}_{\mathrm{f},2}\frac{\partial p_0}{\partial r}\right] = \frac{4}{3} Pr\left[\frac{\partial}{\partial r}\left(\bar{u}_2 + \bar{r}_{\mathrm{f},2}\frac{\partial u_0}{\partial r}\right)\right], \tag{41}$$

$$\left[\overline{T}_2 + \bar{r}_{\mathrm{f},2}\frac{\partial T_0}{\partial r}\right] = \left[\overline{Y}_{\mathrm{F},2} + \bar{r}_{\mathrm{f},2}\frac{\partial Y_{\mathrm{F},0}}{\partial r}\right] = \left[\overline{Y}_{\mathrm{O},2} + \bar{r}_{\mathrm{f},2}\frac{\partial Y_{\mathrm{O},0}}{\partial r}\right] = 0, \tag{42}$$

$$\left[\frac{\partial \overline{T}_2}{\partial r}+\bar{r}_{f,2}\frac{\partial^2 T_0}{\partial r^2}+Le_F^{-1}\left(\frac{\partial \overline{Y}_{F,2}}{\partial r}+\bar{r}_{f,2}\frac{\partial^2 \overline{Y}_{F,2}}{\partial r^2}\right)\right]=0,$$
$$\left[\frac{\partial \overline{T}_2}{\partial r}+\bar{r}_{f,2}\frac{\partial^2 T_0}{\partial r^2}+Le_O^{-1}\left(\frac{\partial \overline{Y}_{O,2}}{\partial r}+\bar{r}_{f,2}\frac{\partial^2 \overline{Y}_{O,2}}{\partial r^2}\right)\right]=0. \quad (43)$$

The values in the far field, $r \to \infty$, are:

$$\bar{u}_2=\bar{v}_2=\bar{p}_2=\overline{T}_2=\overline{Y}_{O,2}\to 0. \quad (44)$$

The solutions to Eqs. (27)–(31) were sought numerically using the boundary value problem solver, COLSYS [16]. This routine employs a collocation method and is capable of solving mixed-order systems of ordinary differential equations, whose boundary values can also be specified at internal points. The latter feature is essential since the jump conditions, as expressed in Eqs. (38)–(43), are prescribed inside the computational domain.

Noting that the unknown variables, $\bar{u}_2$, $\bar{v}_2$, $\bar{p}_2$, $\overline{T}_2$, $\overline{Y}_{F,2}$, and $\overline{Y}_{O,2}$, are discontinuous across the reaction sheet located at $r=r_{f,0}$, these variables are split into two independent variables so that they are continuous throughout the entire domain and their solutions can be readily obtained with the imposed boundary conditions. The solutions corresponding to $r<r_{f,0}$ and $r>r_{f,0}$ are, respectively, denoted by the superscripts "−", and "+". Thus the governing equations can be expressed as a system of 16 first-order differential equations for the 16 unknowns

$$\bar{u}_2^-,\quad \bar{v}_2^-,\quad \frac{\partial \bar{v}_2^-}{\partial r},\quad 4Pr\frac{\partial \bar{u}_2^-}{\partial r}-3\bar{p}_2^-,\quad \overline{T}_2^-,\quad \frac{\partial \overline{T}_2^-}{\partial r},$$
$$\overline{Y}_{F,2}^-,\quad \frac{\partial \overline{Y}_{F,2}^-}{\partial r},\quad \bar{u}_2^+,\quad \bar{v}_2^+,\quad \frac{\partial \bar{v}_2^+}{\partial r},\quad 4Pr\frac{\partial \bar{u}_2^+}{\partial r}-3\bar{p}_2^+,$$
$$\overline{T}_2^+,\quad \frac{\partial \overline{T}_2^+}{\partial r},\quad \overline{Y}_{O,2}^+,\quad \frac{\partial \overline{Y}_{O,2}^+}{\partial r}.$$

Note that there are a total of 17 boundary conditions. The extra boundary condition is needed to determine the perturbed flame location $\bar{r}_{f,2}$, which can be expressed as a function of $\overline{Y}_{F,2}$ by using Eq. (42).

3. Results and discussion

Results and discussions will be presented sequentially for the droplet and burner flames. For each case we shall discuss the effects of variable density by contrasting results obtained by the constant- and variable-density formulations. In order to assess the change in the flame response when the constant-density assumption is removed, numerical solutions of the constant-density formulation were also obtained by suppressing the terms that are due to the density variation. These constant-density solutions were found to be identical to the analytical solutions of [13], thereby validating the numerical solution in this particular limit. Consequently, the following comparisons on the variable-density (*VD*) and constant-density (*CD*) results are based on the numerical solutions.

3.1. Droplet flames

In Fig. 2a, representative profiles of $\bar{u}_2$, $\bar{v}_2$ and $\overline{T}_2$ are plotted for typical droplet burning conditions in a practical combustion environment in that the ambient temperature is greater than the boiling point of a typical liquid fuel, namely that of octane which is 125 °C. Thus a value of $T_s=0.3$ was used. The solid and dotted lines are the solutions of the *VD* and *CD* formulations, respectively. It is seen that the profiles of $\bar{u}_2$, $\bar{v}_2$, and $\overline{T}_2$ are qualitatively similar for these two formulations, with the perturbed variables reaching a maximum value near the rotating surface and then decaying in the far field. Quantitatively, however, their respective magnitudes increase as density is allowed to vary.

The jumps or discontinuities across the profiles shown in Fig. 2 are due to the perturbation that is also applied to r_f.

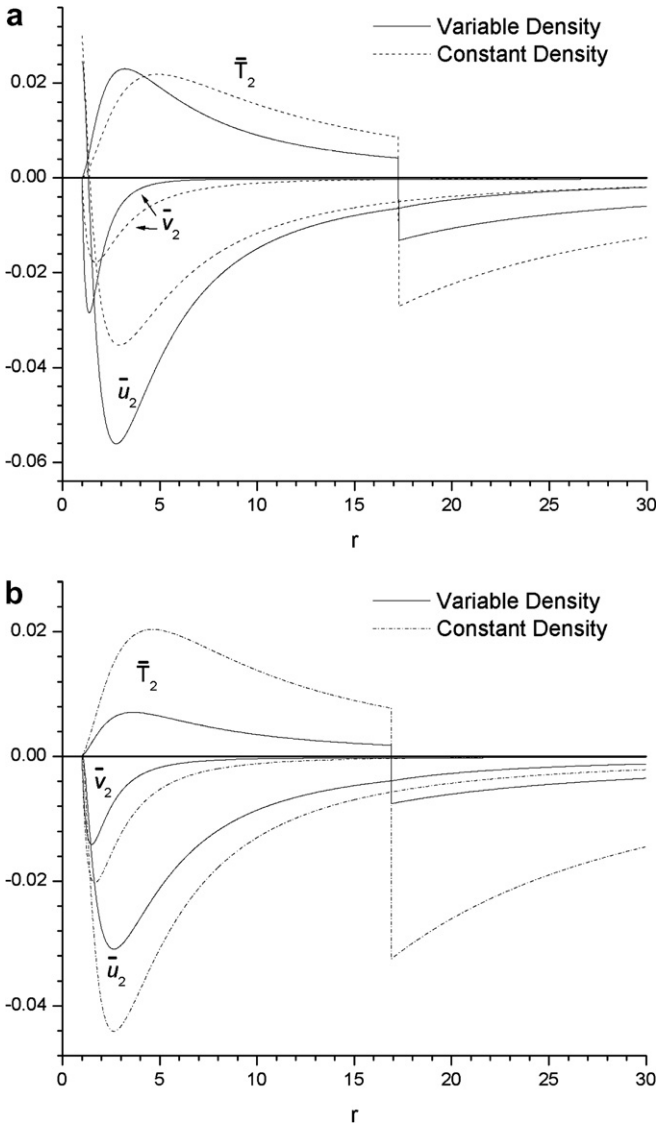

Fig. 2. Radial profiles of $\bar{u}_2$, $\bar{v}_2$, $\overline{T}_2$ for droplet flame at $L=0.1$, $q=12.0$, $Pr=0.7$, $Le_F=Le_O=1.0$, $Y_{O,\infty}=0.23$, (a) $T_s=0.3$, (b) $T_s=1.0$.

Specifically, such perturbations lead to the coupling of the perturbed state variables to $\bar{r}_{f,2}$ and the gradients of T and Y_i across the flame sheet as shown below for the flame temperature:

$$\overline{T}_{f,2} = \overline{T}_2\big|_{r=r_{f,0}} + \left.\frac{\partial T_0}{\partial r}\right|_{r=r_{f,0}} (r_{f,2}).$$

This leads to jumps in perturbed state variables even though each of them is continuous as stated in Eq. (9).

To further assess the influence of density variation, and recognizing that typical droplet experiments conducted in the laboratory involve an isolated droplet in room temperature, additional calculations were conducted for a colder environment, at $T_s = 1.0$, and the results are shown in Fig. 2b. It is seen that, compared to the $T_s = 0.3$ case, while reduction in the magnitude of the profiles for the *CD* formulation is hardly noticeable, the reduction is substantial for the *VD* formulation. Specifically, as T_s decreases the overall magnitude of the perturbed profile increases for the *VD* formulation whereas they remain almost constant for the *CD* formulation. Such a flame response can be explained as follows. As the temperature is raised, the density decreases, which in turn results in a reduction in the momentum transfer of the rotational motion of the burner. Because the driving force for the current system is the viscous transfer of momentum induced by the droplet/burner, a decrease in density inevitably results in an overall decrease in the induced motion as well as the perturbed temperature and species concentrations. Notice that Eqs. (28) and (29), which govern the perturbed velocities, are driven by the source term expressed as the product of the leading-order density (ρ_0) and $\bar{w}_1^2$, which mathematically state how the perturbations induced by the rotating surface is proportional to the density. This can be readily verified by plotting the perturbed profiles for different T_s and will be demonstrated in the next section, where it is shown that burner-supported flames also exert a similar behavior.

The above result is further illustrated in Fig. 3a and b, where the perturbed flame temperature normalized by the leading-order flame temperature, $\overline{T}_{f,2}/T_{f,0}$ is plotted as a function of T_s for the two formulations. We choose to show the fractional perturbation to the flame temperature since it is an important parameter controlling flame extinction and is a physical parameter that can be readily measured experimentally. It is then seen that for the *CD* formulation shown in Fig. 3a, $\overline{T}_{f,2}/T_{f,0}$ is almost independent of T_s, except for the case where Le_F deviates from unity. In contrast, it decreases significantly for the variable density as T_s is increased for all *Le*'s, as shown in Fig. 3b. It is clear at this stage that in the *VD* formulation, the perturbations are expected to increase as T_s decreases as explained previously. It is of interest to note that the magnitude of the profiles predicted by the *CD* formulation is greater than that by the *VD* formulation overall. Physically this is reasonable because the density variation may act as a "buffer" to absorb perturbations due to the rotational

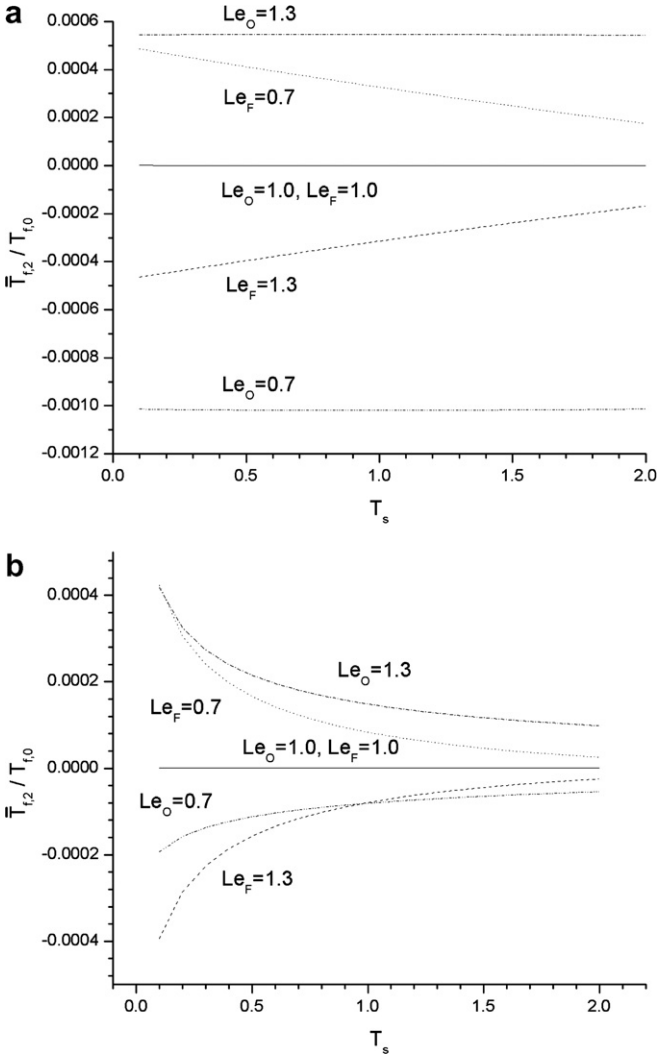

Fig. 3. Fractional flame temperature perturbation $\overline{T}_{f,2}/T_{f,0}$ as function of droplet surface temperature, T_s with different Lewis numbers Le_F and Le_O for the droplet flame ($Y_{O,\infty} = 0.2$, $Pr = 0.7$, $q = 12.0$, $L = 0.1$) obtained by: (a) constant-density, (b) variable-density formulation.

motion. In other words, the propensity of the system to absorb perturbations introduced by the rotational motion is higher when the density is allowed to vary.

The fractional perturbations of the flame radius, $\bar{r}_{f,2}/r_{f,0}$, and temperature, $\overline{T}_{f,2}/T_{f,0}$, from the droplet surface due to rotation are shown as functions of the ambient oxidizer concentration, $Y_{O,\infty}$ in Figs. 4 and 5, respectively. Each of these figures consists of two subplots denoted by (a) and (b), which, respectively, refer to solutions generated by the *CD* and *VD* formulations.

The results show that the flame response due to the rotational perturbation is described well by both formulations. Specifically, the fractional perturbation of the flame radius, $\bar{r}_{f,2}/r_{f,0}$, is negative, regardless of the values of $Y_{O,\infty}$, Le_F and Le_O. The resulting deformed flame surface thus assumes the shape of a pancake, flattened at the poles and protruding outward at the equator. Here the induced secondary flow effectively brings the oxidizer from the ambience toward the poles and then carries it away from

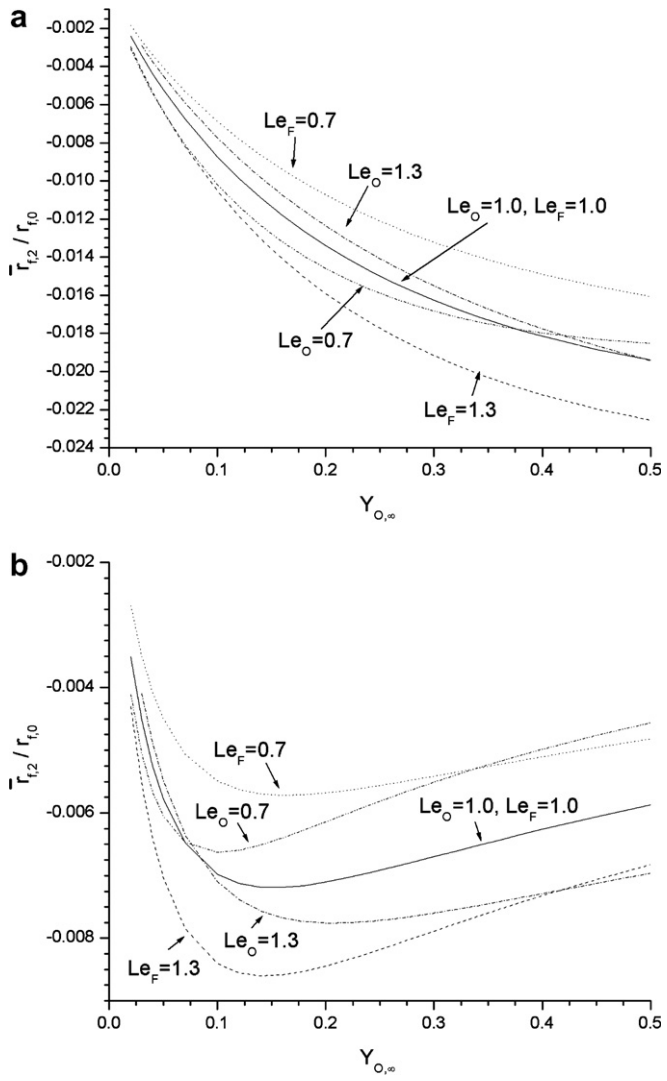

Fig. 4. Fractional flame radius perturbation $\bar{r}_{f,2}/r_{f,0}$ as function of $Y_{O,\infty}$, with different Lewis numbers Le_F and Le_O for the droplet flame ($T_s = 0.3$, $Pr = 0.7$, $L = 0.1$, $q = 12.0$) obtained by: (a) constant-density, (b) variable-density formulation.

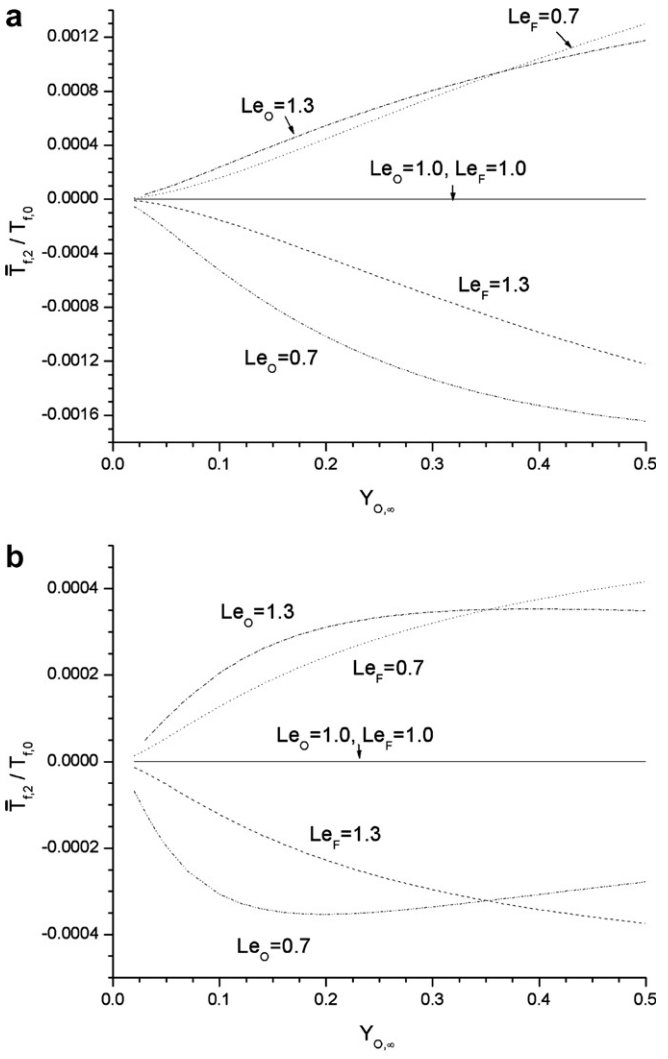

Fig. 5. Fractional flame temperature perturbation $\overline{T}_{f,2}/T_{f,0}$ as function of $Y_{O,\infty}$ with different Lewis numbers Le_F and Le_O for the droplet flame ($T_s = 0.3$, $Pr = 0.7$, $L = 0.1$, $q = 12.0$) obtained by: (a) constant-density, (b) variable-density formulation.

the equator. So the flame surface moves toward the poles but away from the equator in order to achieve stoichiometric burning at the flame surface.

Second, the sign of the fractional flame temperature perturbation, $\overline{T}_{f,2}/T_{f,0}$, in response to changes in $Y_{O,\infty}$ for different Le_F and Le_O is also the same for both formulations. Note that when $Le_F = Le_O = 1$, the flame temperature is not affected ($\overline{T}_{f,2} = 0$) for both formulations as it is only a consequence of the requirement of energy conservation for fuel vaporization at the droplet surface. When the Lewis numbers deviate from unity, an additional effect is present, namely the combination of preferential mass or thermal diffusion with flame stretch. Both formulations predict an increase in the flame temperature at the poles ($\overline{T}_{f,2} > 0$) for $Le_F < 1$ (and $Le_O = 1$) or $Le_O > 1$ (and $Le_F = 1$), and a decrease in the flame temperature when the Le's are reversed.

In summary, while the response of the flame is largely described by the *CD* formulation, important and substantial differences exist between its predictions and those of the *VD* formulation. First, the overall magnitude of the perturbations is over-predicted by the *CD* formulation. Consequently, the overall magnitudes of both the flame location and temperature perturbations are substantially smaller when the *CD* assumption is removed. Second, the perturbations are no longer monotonic for the droplet flames when the density is varied, as shown in Figs. 4 and 5.

3.2. Burner-generated flames

Here we first note that the only difference between the droplet and burner formulations is in the two boundary conditions specified at the rotating surface: (1) the mass flux is specified and not perturbed for the burner-generated

flame, while it is perturbed for the droplet flame, as shown in Eqs. (37a) and (37b), (2) a higher ambient temperature is specified for droplet burning, resulting in $T_s < 1$, while it is at a lower value, typically the room temperature, for the burner-supported flame, with $T_s \geqslant 1$.

The profiles for a typical burner-supported flame are shown in Fig. 6a, which exhibit similar trends as those shown in Fig. 2b except that $\bar{u}_2$ vanishes at the surface. This is in accordance with observations made in our preliminary experiments conducted in microgravity, in which the flame standoff distance was kept sufficiently far away from burner surface in order to minimize heat loss to the burner. Similar to the droplet case, the profiles obtained from both formulations agree qualitatively, but the magnitude of the perturbations decrease when density is allowed to vary. It is further seen in Fig. 6b that, for $T_s = 0.3$, the profiles for the variable-density formulation increase substantially while those for the constant-density formulation increase only slightly, resulting in much larger perturbations. This in fact is the same for the droplet case (see Fig. 2a and b). Hence, it is evident that perturbations increase (decrease) with decreasing (increasing) T_s and the trend is independent of the burning modes.

The above observation can be further illustrated by plotting $\overline{T}_{f,2}/T_{f,0}$ as a function of T_s, similar to those shown in Fig. 3. Since the response is qualitatively similar to that of the droplet cases, they are not shown here. Instead, the profiles for different T_s are depicted in Fig. 7a and b, where perturbed velocity and temperature profiles are shown, respectively, for both formulations. We first note that the profiles shown in Fig. 7a obtained by the *CD* formulation remain the same for all T_s because momentum is decoupled from the energy equation. In fact, although not shown, profiles of $\bar{v}_2$, $\overline{Y}_{F,2}$, and $\overline{Y}_{O,2}$ all remain unchanged with variations of T_s. In contrast, a significant increase in the magnitude of profiles is obtained for the *VD* formulation

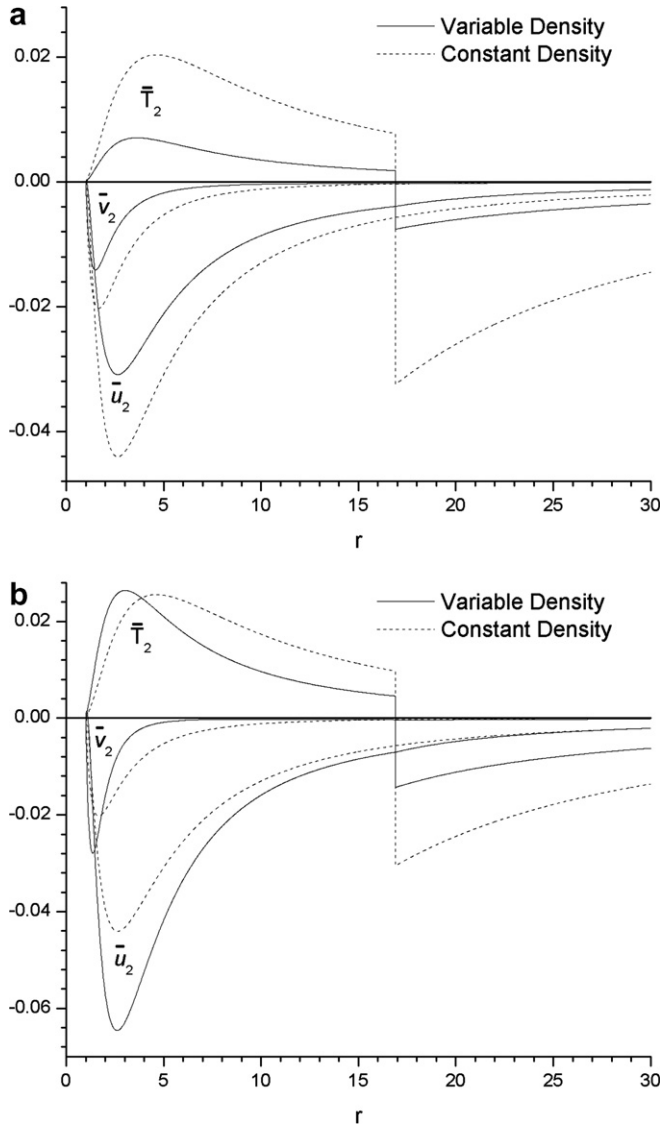

Fig. 6. Radial profiles of $\bar{u}_2$, $\bar{v}_2$, $\overline{T}_2$ for burner-generated flame at $M_0 = 3.5$, $Pr = 0.7$, $Le_F = Le_O = 1.0$, $Y_{O,\infty} = 0.23$, (a) $T_s = 1.0$, (b) $T_s = 0.3$.

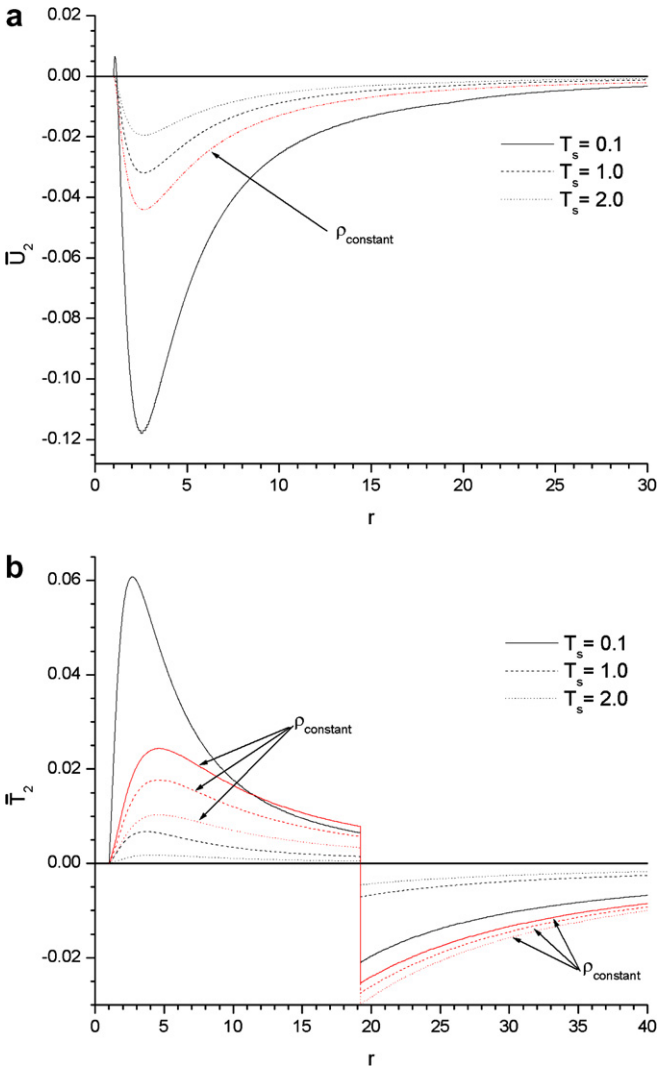

Fig. 7. Radial profiles of (a) $\bar{u}_2$ and (b) $\overline{T}_2$ for burner-generated flames at $T_s = 0.1$, 1.0, and 2.0 ($Pr = 0.7$, $M_0 = 3.5$, $Y_{O,\infty} = 0.2$).

as T_s is decreased. Note that when $T_s = 0.1$, the peak of $\bar{u}_2$ for the *VD* formulation is three times that of the *CD* formulation, which indicates that under such conditions, the *CD* formulation can actually under-predict the effect of rotation. The $\overline{T}_2$ profiles depicted in Fig. 7b also exert similar behavior, except that the profiles obtained from the *CD* formulation now vary similarly as the *VD* formulation. This is due to the fact that $\overline{T}_2$ depends on the leading-order temperature gradient, as shown in Eq. (30), which in turn depends on T_s. The fact that the perturbed temperature profile increases with decreasing T_s even when the density is held fixed, is interesting since this would imply that when coupled with the effect of variable density, such a behavior would be amplified. This is clearly demonstrated in the profiles obtained by the *VD* formulation, where the increase in the magnitude of the profiles is much larger as compared with the growth predicted by the *CD* formulation.

The $\bar{r}_{f,2}/r_{f,0}$ and $\overline{T}_{f,2}/T_{f,0}$ of the burner solution are shown as functions of $Y_{O,\infty}$ in Figs. 8 and 9, respectively. Each figure contains two subplots denoted by (a) and (b), which, respectively, refer to solutions generated by the *CD* and *VD* formulations.

It is seen that while the response of the flame shape is identical to that of the droplet case as shown in Fig. 8a and b, the perturbation to the flame temperature is modified. When $Le_F = Le_O = 1$, the flame temperature decreases at the poles, $\overline{T}_{f,2} < 0$, as shown in Fig. 8. This is due to flattening of the flame surface in the presence of rotation, which in turn increases the heat loss to the burner at the poles and reduces it around the equator. Furthermore, the sign $\overline{T}_{f,2}/\overline{T}_{f,0}$ of in response to changes in $Y_{O,\infty}$ for different Le_F and Le_O is also the same for both formulations. However, this Lewis number effect is modified by heat loss to the burner surface when $Y_{O,\infty}$ becomes sufficiently large

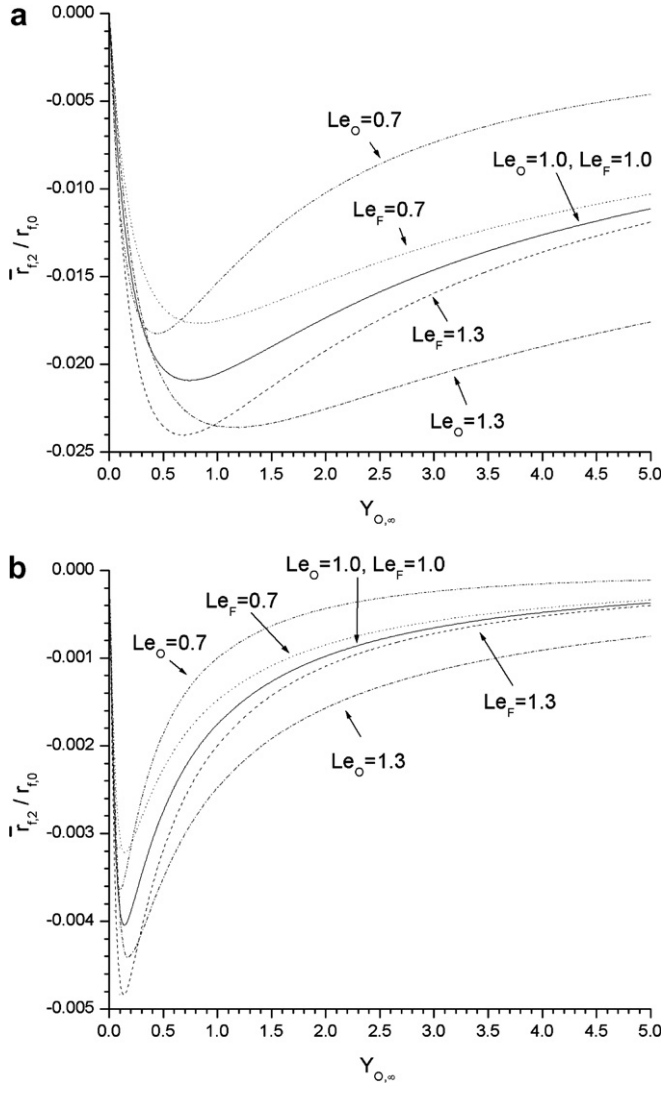

Fig. 8. Fractional flame radius perturbation $\bar{r}_{f,2}/r_{f,0}$ as function of $Y_{O,\infty}$,with different Lewis numbers Le_F and Le_O for the burner-generated flame ($T_s = 1.0$, $Pr = 0.7$, $M_0 = 3.5$) obtained by: (a) constant-density, (b) variable-density formulation.

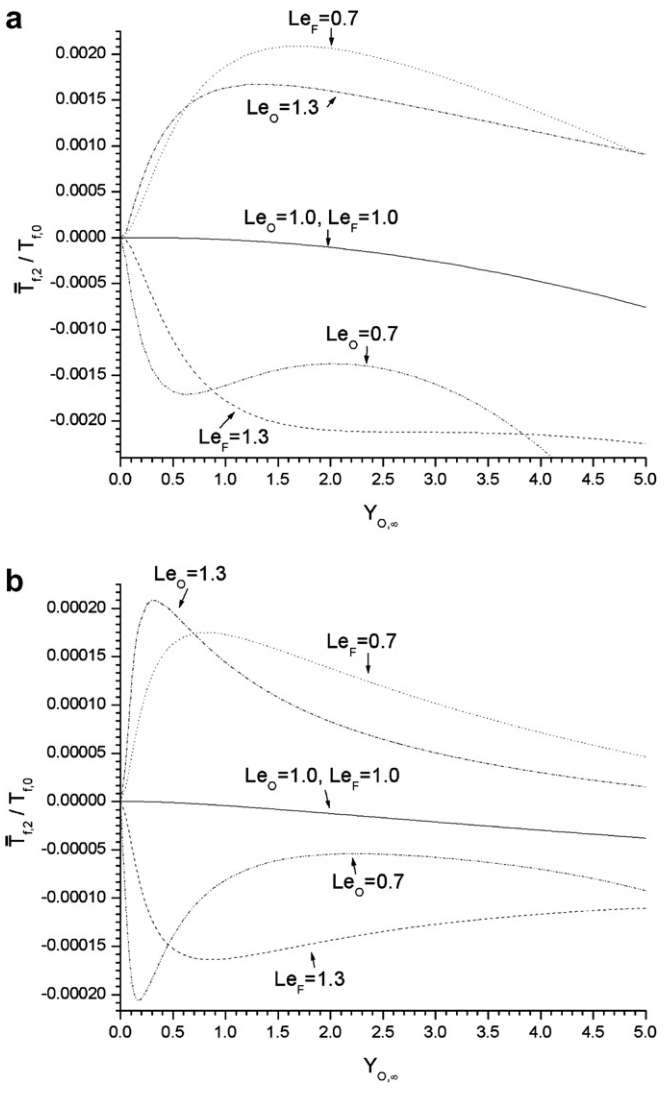

Fig. 9. Fractional flame temperature perturbation $\overline{T}_{f,2}/T_{f,0}$ as function of $Y_{O,\infty}$ with different Lewis numbers Le_F and Le_O for the burner-generated flame ($T_s = 1.0$, $Pr = 0.7$, $M_0 = 3.5$) obtained by: (a) constant-density, (b) variable-density formulation.

so that the flame is situated closer to the burner surface and the extent of heat loss increases. This is clearly demonstrated in Fig. 9, which shows that the perturbed flame temperature for all Lewis numbers eventually decrease to negative values as $Y_{O,\infty}$ increases. Furthermore, since the flame is always flattened at the poles and protrudes outward from the equator, there is greater heat loss at the poles, resulting in negative $\overline{T}_{f,2}$.

Similar to the droplet case, the perturbations associated with the *VD* formulation are small compared to those of the constant density. Second, as shown in Figs. 8 and 9, perturbations decrease rapidly as $Y_{O,\infty}$ increases for the *VD* formulation, whereas they are broadened over a wide range of $Y_{O,\infty}$ with the *CD* formulation. For example, the former predicts that $\bar{r}_{f,2}/r_{f,0}$ is largest around $Y_{O,\infty} = 0.15$ for all Lewis numbers, while the maximum of $\bar{r}_{f,2}/r_{f,0}$ varies over a wider range of $Y_{O,\infty}$ for the latter.

As described earlier, perturbations to the flame temperature eventually decrease as $Y_{O,\infty}$ in creases. This effect appears to be much stronger when the *CD* assumption is removed. In order to gain a clearer picture, we first need to break down the effect of varying $Y_{O,\infty}$. First, we note that as $Y_{O,\infty}$ increases, the flame situates closer to the burner surface and the flame temperature increases, while the opposite holds when $Y_{O,\infty}$ decreases. Second, perturbations to the velocity induced by the rotating burner are localized near the burner (see Figs. 6 and 7). Third, the perturbed velocity profiles are not affected by either the species concentration or the temperature in the constant-density formulation (demonstrated in Fig. 7). In other words, no matter where the flame is located relative to the burner, the induced velocity field is solved independently.

Considering the three points above, we would expect that the coupling between the perturbations to the velocity and temperature fields induced by the rotating burner would be minimal when the flame is located sufficiently far away. In other words, as $Y_{O,\infty}$ becomes extremely small, the induced velocity profiles obtained from the *VD* formulation should approach those obtained from the *CD* formulation. By the same reasoning, as $Y_{O,\infty}$ increases, we would expect to see a stronger coupling between momentum and energy when the flame approaches the burner and eventually penetrate into the region where the velocity perturbation is large. Furthermore, such coupling inevitably results in a rapid reduction of the effects of rotation. Recall that perturbations decrease with increasing T_s, which also results in temperature increase around the rotating surface.

This is clearly demonstrated in Fig. 10, in which perturbed velocity profiles for both formulations are presented for various $Y_{O,\infty}$. Each arrow indicates the leading-order location of the flame for the corresponding $Y_{O,\infty}$. The flame locations are not indicated if they are beyond the scale of the plot. First, it is seen that the perturbed velocity profiles obtained by the *CD* formulation do not depend on $Y_{O,\infty}$, as indicated by a single curve. The flame location is also not indicated since it is identical to the *VD* formulation. Second, the magnitude of the profiles decreases as the lead-

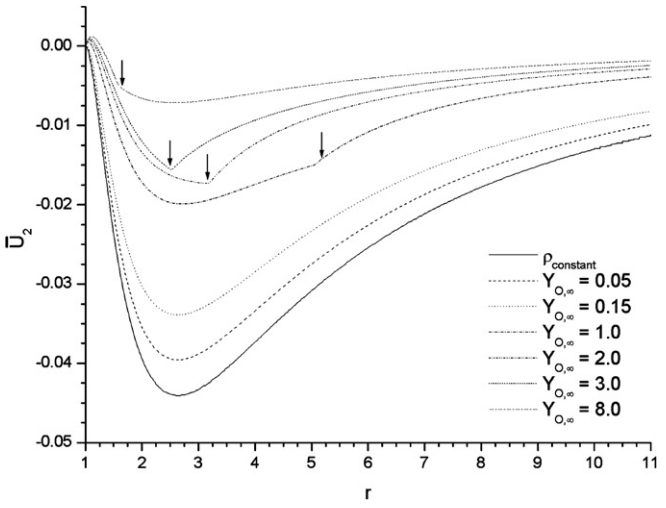

Fig. 10. Radial profiles of $\bar{u}_2$ for burner-generated flames at varying $Y_{O,\infty}$. ($Pr = 0.7$, $M_0 = 3.5$, $T_s = 1.0$).

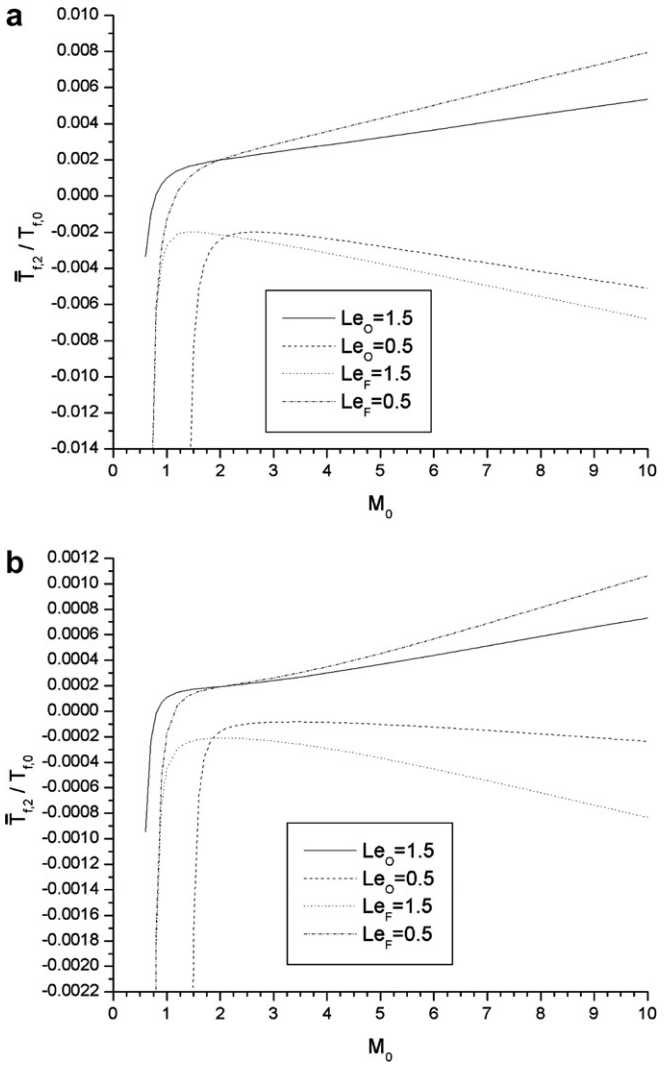

Fig. 11. Fractional flame temperature perturbation $\overline{T}_{f,2}/T_{f,0}$ as function of mass flux for $Le_F = 0.50$ and 2.0, $Le_O = 0.50$ and 2.0 ($T_s = 1.0$, $Pr = 0.7$, $Y_{O,\infty} = 1.0$) obtained by: (a) constant-density, (b) variable-density formulation.

ing-order flame location moves towards the burner surface with increasing $Y_{O,\infty}$. Lastly, the *VD* profiles approach those of the *CD* formulation as $Y_{O,\infty}$ decreases, resulting in larger flame stand-off distance.

Finally, Fig. 11a and b compares the effects of M_O on $\overline{T}_{f,2}/T_{f,0}$ for different values of Le_O and Le_F for the two formulations, with $Y_{O,\infty}$ held fixed at 1.0 and only the mass flux is varied. It is seen that for very small M_O, the flame is so close to the burner that heat loss dominates, resulting in large negative values of $\overline{T}_{f,2}/T_{f,0}$, which agrees with the previous observation. With a slight increase in M_O, the heat loss to the burner decreases and $\overline{T}_{f,2}/T_{f,0}$ rapidly increases. As M_O is increased beyond 1.5, the flame stand-off distance becomes sufficiently large such that the influence of heat loss to the burner diminishes and that due to non-unity *Le* takes over. As a result, $\overline{T}_{f,2}/T_{f,0}$ starts to decreases again for $Le_F = 2.0$ ($Le_O = 0.5$), whereas it increases steadily for $Le_F = 0.5$ ($Le_O = 2.0$) until it becomes positive, which is also shown in Fig. 9. The major difference introduced by the *VD* formulation is again the smaller perturbations and the nonlinear variation of $\overline{T}_{f,2}/T_{f,0}$ with M_O.

4. Concluding remarks

In our previous work [12], by assuming constant density a perturbation analysis was carried out to examine effects of the secondary flow induced by rotation on the response of spherical diffusion flames enveloping either a burner or a fuel droplet. Complete analytical solutions were found for all the relevant quantities, with explicit expressions derived for the burning rate and distorted flame shape. General Lewis numbers were considered, as were ambient oxidizer concentration. The effect of rotation on local extinction was also assessed.

While the constant-density assumption simplifies the analysis considerably by decoupling the flow from the thermal effects and provides elegant analytical results, such a simplification is known to yield incorrect flame locations compared to experimental results as mentioned in the introduction. One could possibly argue that density variation offers the flexibility for the system to absorb perturbing effects as compared to a constant-density flow, which is more rigid and tends to manifest any perturbation directly. However, it is also possible that thermal expansion effects will magnify the effects of rotational perturbations. To address this, we carried out the analysis without making the constant-density assumption and the solutions were obtained numerically.

The key findings of our previous work still hold. When the otherwise spherical diffusion flame front is subjected to axial rotation, the flame is distorted into a pancake shape flattened at the poles but protruding at the equator, consistent with our experimental findings [3]. The rotation also affects the flame temperature by altering the extent of heat loss and flame stretch. For unity Lewis numbers, the flame stretch effect is absent and the response is only controlled by the heat loss to the surface. The flame from the burner experiences temperature reduction (enhancement) at the poles (equator) as more (less) heat is lost to the surface by the flame deformation. The flame temperature from the fuel droplet, however, does not change because of energy conservation for the droplet vaporization process.

With $Le_F > 1$ or $Le_O < 1$, both flames from the burner and droplet experience temperature reduction at the poles but elevation at the equator. As the Lewis numbers change to the values of $Le_F < 1$ or $Le_O > 1$, the sign of $\overline{T}_{f,2}$ for the flame from the burner is also affected by the ambient oxidizer concentration, $Y_{O,\infty}$. The flame temperature then increases at the poles and decreases at the equator when $Y_{O,\infty}$ is small. As $Y_{O,\infty}$ increases, the flame temperature decreases at the poles but increases at the equator because, at such high $Y_{O,\infty}$, the flame is so close to the burner that heat loss to the burner dominates over *Le* effects. For droplet burning with $Le_F < 1$ or $Le_O > 1$, the sign of $\overline{T}_{f,2}$ is not affected by $Y_{O,\infty}$, $\overline{T}_{f,2}$ is positive and the flame temperature increases at the poles but decreases at the equator.

Furthermore, since our flame structure analysis [13] is general, it is still true that the flame temperature perturbations due to rotation can result in local extinction because of the temperature-sensitive Arrhenius kinetics. In other words, the flame can extinguish locally around the region where the rotation causes the greatest reduction of the flame temperature. Local extinction will therefore first occur either at the poles or the equator, depending on the values of Lewis number and ambient oxidizer concentration.

We have also gained new insights into the current problem when the density variation is fully taken into account. It is found that the magnitude of the perturbations depended strongly on the ratio of the burner/droplet surface and the ambient, denoted by T_s. While the perturbations decrease significantly when $T_s > 1$, the magnitude is comparable to that predicted by the *CD* formulation when $T_s < 1$. This implies that the effect of rotation reported here is significant only when the ambient temperature is high compared to that of the droplet/burner surface. Nevertheless, such effects are observable for near-limit situations in which flame extinction can be readily triggered with slight temperature perturbations.

Acknowledgements

It is a pleasure to acknowledge stimulating discussions with Prof. John K. Bechtold of the New Jersey Institute of Technology during the course of this investigation. This research was supported by the microgravity combustion program and a GSRP fellowship of NASA, under the technical monitoring of Dr. Kurt Sacksteder.

References

[1] H. Tsuji, Counterflow diffusion flames, Prog. Energy Combust. Sci. 8 (1982) 93–119.

[2] C.J. Mueller, J.F. Driscoll, D.L. Ruess, M.C. Drake, Effects of unsteady stretch on the strength of a freely propagating flame wrinkled by a vortex, Proceedings of the Combustion Institute, vol. 26, The Combustion Institute, Pittsburg, PA, 1996, pp. 347–355.
[3] S.W. Yoo, On the structure and dynamics of stationary and rotating spherical diffusion flames, Ph.D. Thesis, Princeton University, Princeton, New Jersey, 2006.
[4] W.G. Bickley, The secondary flow due to a spherical rotating in a viscous fluid, Philos. Mag. 25 (7th Series) (1938) 746–752.
[5] H. Takagi, Viscous-flow induced by slow rotation of a sphere, J. Phys. Soc. Jpn. 42 (1977) 319–325.
[6] L. Howarth, Note on the boundary layer on a rotating sphere, Philos. Mag. 42 (7th Series) (1951) 1308–1315.
[7] S.N. Singh, Laminar boundary layer on a rotating sphere, Phys. Fluids 13 (1970) 2452–2454.
[8] S.C.R. Dennis, D.B. Ingham, S.N. Singh, The steady flow of a viscous fluid due to a rotating sphere, J. Fluid Mech. 34 (1981) 361–381.
[9] O. Sawatzki, Flow field around a rotating sphere, Acta Mech. 9 (1970) 159–214.
[10] H.G. Pearlman, S.H. Sohrab, The role of droplet rotation in turbulent spray combustion modeling, Combust. Sci. Technol. 76 (1991) 321–334.
[11] D. Lozinski, M. Matalon, Vaporization of a spinning fuel droplet, Proceedings of the Combustion Institute, vol. 24, The Combustion Institute, Pittsburg, PA, 1992, pp. 1483–1491.
[12] D. Lozinski, M. Matalon, Combustion of a spinning fuel droplet, Combust. Sci. Technol. 96 (1994) 345–367.
[13] S.W. Yoo, J. Qian, J.K. Bechtold, C.K. Law, Response of spherical diffusion flames under rotation with general Lewis numbers, Combust. Theor. Model. 9 (2005) 199–217.
[14] M. Klajn, A.K. Oppenheim, Influence of exothermicity on the shape of a diffusion flame, Proceedings of the Combustion Institute, vol. 19, The Combustion Institute, Pittsburg, PA, 1982, pp. 223–235.
[15] C.K. Law, Combustion Physics, Cambridge, 2006.
[16] U. Ascher, J. Christiansen, R.D. Russel, Collocation software for boundary-value ODEs, ACM Trans. Math. Software 7 (1981) 209–222.